



Probing the in-air growth of large area of 3D functional structures into a 2D supramolecular nanoporous network

Romain Brisse, Dominique Guianvarc'H, Christelle Mansuy, Sandrine Sagan, David Kreher, Lydia Sosa-Vargas, Lydia Hamitouche, Vincent Humblot, Imad Arfaoui, Vanessa Labet, et al.

► To cite this version:

Romain Brisse, Dominique Guianvarc'H, Christelle Mansuy, Sandrine Sagan, David Kreher, et al.. Probing the in-air growth of large area of 3D functional structures into a 2D supramolecular nanoporous network. Chemical Communications, 2018, 54 (72), pp.10068-10071. 10.1039/c8cc06125d . hal-01969600

HAL Id: hal-01969600







<https://hal.sorbonne-universite.fr/hal-01969600>

Submitted on 4 Jan 2019

HAL is a multi-disciplinary open access archive for the deposit and dissemination of scientific research documents, whether they are published or not. The documents may come from teaching and research institutions in France or abroad, or from public or private research centers.

L'archive ouverte pluridisciplinaire **HAL**, est destinée au dépôt et à la diffusion de documents scientifiques de niveau recherche, publiés ou non, émanant des établissements d'enseignement et de recherche français ou étrangers, des laboratoires publics ou privés.

Probing the in-air growth of large area of 3D functional structures into a 2D supramolecular nanoporous network†

Romain Brisse, ^{abc} Dominique Guianvarc'h, ^b Christelle Mansuy, ^b
Sandrine Sagan, ^b David Kreher,^a Lydia Sosa-Vargas, ^a Lydia Hamitouche,^a
Vincent Humblot, ^d Imad Arfaoui, ^c Vanessa Labet, ^c Céline Paris,^c
Christophe Petit ^{*c} and André-Jean Attias ^{*ae}

Surface-confined host–guest chemistry at the air/solid interface is used for trapping a functionalized 3D Zn–phthalocyanine complex into a 2D porous supramolecular template allowing the large area functionalization of an sp^2 -hybridized carbon-based substrate as evidenced by STM, resonance Raman spectroscopy, and water contact angle measurements.

Supramolecular self-assembly of building blocks (tectons) at surfaces has emerged as a powerful tool to pattern well-organized monolayers on the nanoscale.¹ The formation of two-dimensional (2D) supramolecular nanostructures is achieved either under ultra-high vacuum (UHV) or at the liquid/solid interface.² To go beyond the well-mastered decorative 2D supramolecular self-assembly, the next challenge is the realization by an easy process of large functional surfaces in view of practical applications.³

Regarding the issue of dealing with functionalization, two main strategies have been developed: (i) forming 2D surface-confined supramolecular nanoporous networks and taking advantage of their potential for hosting guests and confined phenomena.⁴ Several functionalities have been evidenced, ranging from the selective adsorption of guest molecules,⁵ to the guest-induced hierarchical (multicomponent) nanostructures,⁶ control of the dynamic properties of trapped species,⁷ site-selective immobilization of guest molecules in periodically functionalized host cavities,⁸ photo-responsive host–guest systems,⁹ and cavity-confined supramolecular coordination.¹⁰ However, since the above

works focused only on 2D components, the interactions with the environment are limited to the upper surface. (ii) This is why to go further in the functionalization, it is mandatory to develop interactions in the dimension perpendicular to the surface.¹¹ To address this issue, several approaches have been proposed, based on covalent or noncovalent 3D structures able to project into the third dimension, displaying a functionality. Regarding the covalent 3D tectons, we can mention the triazatriangulonium ion (TATA)-based platform¹² and Janus tecton platform¹³ developed for possible applications in the fields of molecular machines and photonics, respectively. With respect to noncovalent tectons, porphyrins (P) and phthalocyanines (Pc) are interesting building blocks for obtaining surface-confined self-assembly of 3D functional tectons by metal complexation or axial ligation.¹⁴ Indeed, it has been demonstrated that the macrocycle unit predominantly adsorbs parallel to the substrate plane, whereas the coordination allows for the projection in the direction perpendicular to the substrate plane. This has been reported for multi-decker lanthanide porphyrin/phthalocyanine sandwich complexes explored as molecular magnets and rotors on the one hand,¹⁵ and zinc porphyrin (ZnP) derivatives coordinated with a pyridine-based axial ligand (4-methoxypyridine, or 3-nitropyridine) on the other hand.¹⁶ Among all the above approaches, mounting on a metalated tetrapyrrole macrocycle an appropriately functionalized axial ligand appears very promising due to the versatile character and ease of the coordination reaction. However, the macrocycles were derivatized to steer the supramolecular self-assembly on the substrate on the one hand, and the coordination occurred on an already metallo-P covered surface on the other hand.

In previous works,¹⁷ we demonstrated that 1,3,5-tristyrylbenzene derivatives substituted in positions 3 and 5 by alkoxy peripheral chains presenting n carbon atoms (TSB3,5- C_n) (Scheme S1, ESI†) are able to form, at the liquid/solid interface, by van der Waals interactions between the alkyl chains on highly oriented pyrolytic graphite (HOPG), surface-confined nanoporous honeycomb networks able to act as 2D molecular sieves. More particularly, it was shown that underivatized phthalocyanine (Pc) could be immobilized in the TSB3,5- C_{12}

^a IPCM, UMR CNRS-Sorbonne Université 8232, 4 Place Jussieu, 75005 Paris, France.

E-mail: andre-jean.attias@sorbonne-universite.fr

^b Sorbonne Université, École Normale Supérieure, PSL University, CNRS,

Laboratoire des biomolécules, LBM, 75005 Paris, France

^c MONARIS, UMR CNRS-Sorbonne Université 8233, 4 Place Jussieu, 75005 Paris,

France. E-mail: christophe.petit@sorbonne-universite.fr

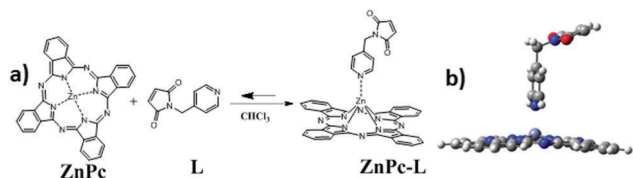
^d LRS, UMR CNRS-Sorbonne Université 7197, 4 Place Jussieu, 75005 Paris, France

^e UMI Building Blocks for Future Electronics, CNRS – Sorbonne Université – Yonsei

University – Ewha Womans University, 50 Yonsei-ro Seodaemun-gu, Seoul, Korea.

E-mail: aj-attias@yonsei.ac.kr

† Electronic supplementary information (ESI) available: Synthetic details, experimental details, Raman spectroscopy, DFT modeling, and WCA images. See DOI: 10.1039/c8cc06125d



Scheme 1 (a) Complexation of **ZnPc** with **L** in chloroform and (b) modeling of the chemical structure of the complex by DFT calculations (see the ESI†).

cavities.¹⁸ Therefore, we propose to combine the cavity surface-confined host-guest recognition and the metallo-Pc axial ligation approaches to immobilize standing-up 3D functional guest structures into the voids of a 2D host template.¹⁹ Moreover, we provide a way for large area patterning and the associated characterization on different scales in air.

Here, we report the growth, by a drop-casting method at the air/HOPG interface, of large area (up to mm^2) 3D structures from a 2D porous template and the multiscale characterization by scanning tunneling microscopy (STM), Raman spectroscopy, and contact angle measurements. With this aim, we first synthesized a 3D functional tecton (**ZnPc-L**) consisting of a pyridine-based ligand (**L**) functionalized with a maleimide function and mounted on a Zn-phthalocyanine (**ZnPc**) (Scheme 1). The maleimide function was chosen to allow further thiol-Michael addition click reaction widely used for biomolecular synthesis and labelling of biomolecules.²⁰ Our large area patterning process consists of the following sequences: growth of an ordered 2D porous network by drop-casting from a **TSB3,5-C₁₂** solution in chloroform (CHCl_3), solvent evaporation, and subsequent drop-casting, on the dry host network film, of a 3D **ZnPc-L** solution in CHCl_3 , to finally trap them in the template pores. For comparison, similar experiments were performed with planar **ZnPc**. After evaporation of the solvent, STM images at the air/HOPG interface only provide information of the functionalized surface organization. Therefore, to get some chemical information about the **TSB3,5-C₁₂** pores filling with **ZnPc** or **ZnPc-L** molecules, the present work explores the use of Raman spectroscopy and contact angle measurements. By combining all the above techniques as well as DFT calculations, we demonstrate that the 3D tectons build up perpendicular to the substrate projecting the maleimide function in a parallel plane above the surface. Unexpectedly, the adlayer hydrophilicity can be tuned depending on the guest molecules.

As an axial ligand, we initially targeted *N*-(4-pyridyl)maleimide by reacting maleimide with 4-aminopyridine (Scheme S2a, ESI†).²¹ However, this attempt failed due to the propensity of maleic anhydride to polymerize in the presence of pyridine.²² Protecting the maleimide double bond, *via* the well-known thermoreversible Diels-Alder (DA) reaction,²³ gave also unreproducible results and did not permit prevention of the polymerization reaction (Scheme S2b, ESI†), which could be promoted by the high basicity of the pyridine ring in 4-aminopyridine ($\text{p}K_{\text{a}} = 9.2$). This is why the ligand **L** was targeted (Scheme S3, ESI†), the synthetic route combines the use of the less basic 4-aminomethylpyridine ($\text{p}K_{\text{a}} = 4.3$) with the protection/deprotection of the maleimide double bond *via* a DA/retro-DA reaction (see Experimental details in the ESI†).

The coordination of **ZnPc** with ligand **L** was operated in solution and monitored by UV/visible spectroscopy (Fig. S1, ESI†). Chloroform was chosen as the solvent, owing to its poorly coordinating capabilities and so as to maximize the coordination rate of **L** with **ZnPc**.²⁴ The obtained solution contained monomeric **ZnPc** as evidenced by the shape of the UV-visible spectrum (sharp Q-band at 671 nm and absence of H or J shoulders).²⁵ The progressive addition of aliquots of **L** to the **ZnPc** solution induced batho- and hypochromic effects of the Zn-Pc Q-band. In agreement with the literature,²⁶ this was attributed to the formation of the **ZnPc-L** complex. Saturation was reached at about 150 eq., confirming the formation of the **ZnPc-L** complex with the maximum rate.

In view of potential applications, it is necessary to prove the functionalization on a large scale. To address this issue, the use of complementary techniques is needed. First, the supramolecular self-assembly was investigated by STM. To circumvent the complexification induced by working under UHV or at the liquid/solid interface, large-scale ($200 \times 200 \text{ nm}^2$ up to $400 \times 400 \text{ nm}^2$) STM images were recorded at the air/HOPG interface. With this aim, some representative STM images recorded at different spots of the host nanoporous molecular monolayer and the same sized images after the addition of guest molecules, *i.e.* **ZnPc** and **ZnPc-L** molecules, are shown in Fig. 1 and 2.

Fig. 1a reveals that **TSB3,5-C₁₂** molecules form a stable long-range well-ordered 2D honeycomb structure at the air/HOPG interface. Then, it is possible to extract from Fig. 1b unit cell parameters associated to the 2D hexagonal packing ($a = b = 4.2 \text{ nm}$ and $\alpha = 60.0^\circ$). Since they are similar within experimental errors to those reported at the 1-phenyloctane/HOPG interface,¹⁷ the drop-casting process does not affect the lattice parameters.

To demonstrate the trapping of **ZnPc** and its derivatives at the air/solid interface, first **ZnPc** molecules were deposited onto the **TSB3,5-C₁₂** nanoporous monolayer (see the ESI†). Fig. 2a shows a typical STM image where almost the entire honeycomb structure is filled with **ZnPc** molecules, appearing as bright spots. These guest molecules are trapped by the host template and they should lie flat on HOPG. It is also possible to observe some features of the underlying nanoporous molecular monolayer. Note that several areas of the HOPG substrate having also a smaller **ZnPc** coverage rate are observed, probably due the

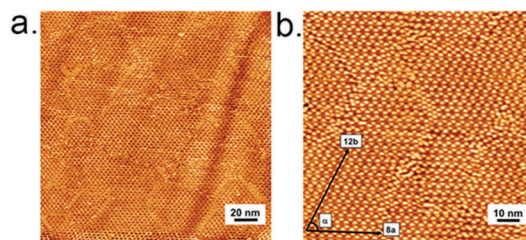


Fig. 1 Well-defined nanoporous monolayer of **TSB3,5-C₁₂** molecules deposited on HOPG by drop-casting. (a) $200 \text{ nm} \times 200 \text{ nm}$ long-range STM image and (b) $100 \text{ nm} \times 100 \text{ nm}$ STM image of the supramolecular self-assembly, recorded at the air/HOPG interface in the current mode with -1.3 V and 15 pA as the sample bias and tunneling current, respectively.

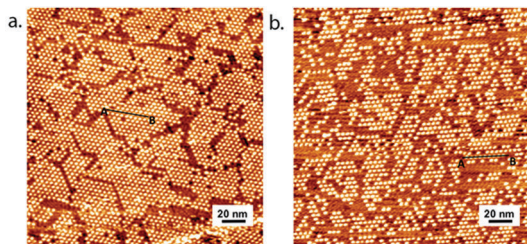


Fig. 2 Nanoporous monolayer of **TSB3,5-C₁₂** molecules after the addition, by drop-casting, of guest molecules: (a) **ZnPc** molecules, 200 nm × 200 nm STM image, (b) **ZnPc-L** complex molecules, 200 nm × 200 nm STM image. All images were recorded at the air/HOPG interface in the current mode with −1.3 V and 12 pA as the sample bias and tunneling current, respectively.

wettability and the fast drying of chloroform inducing local inhomogeneities.

Now, when the same experiment is performed with **ZnPc-L** molecules, again the honeycomb structure is filled as shown in Fig. 2b. From the unit cell area of the nanoporous monolayer (Fig. 1b), *i.e.* 15.3 nm² ($a = b = 4.2$ nm), one deduces that the maximum coverage rate for **ZnPc** or **ZnPc-L** molecules onto the nanoporous monolayer corresponds to 0.065 molecules per nm². Thus, the coverage rate is estimated to be 92% ± 2% and 57% ± 2% for **ZnPc** (Fig. 2a) and **ZnPc-L** (Fig. 2b), respectively. Although **ZnPc-L** molecules are expected to form a protrusion due to the presence of the ligand **L**, cross-sections corresponding to the black line AB (Fig. 2a and b, respectively) show that the apparent heights of **ZnPc** and **ZnPc-L** molecules are similar, ~0.4 nm (Fig. S2, ESI†). At this stage, one can only deduce that the nanoporous template is filled, but it is not possible to distinguish between **ZnPc** and **ZnPc-L** molecules. Indeed, the observed apparent height is due to the electronic density at the Fermi level, although some authors claim that it should be possible to distinguish between similar molecules through deep, long, and tedious STM investigations whose results at the few nanometer scale are debatable.¹⁶

In order to complement the information given by STM measurements, another particular challenge for the fabrication of sophisticated out-of-plane functional surfaces is the chemical characterization of the different components used as building blocks. With this aim, resonance Raman spectroscopy was used to chemically probe the functionalization of the HOPG surfaces. The 633 nm wavelength excitation was chosen, to be in the absorption of the Q band (Fig. S1, ESI†) of **ZnPc** and **ZnPc-L**. Fig. S3 (ESI†) shows the spectra of **TSB3,5-C₁₂** deposited on HOPG, **ZnPc** and **ZnPc-L** deposited inside the **TSB3,5-C₁₂** network, as well as the spectra of pure **ZnPc** and **L** molecules. At 633 nm, the Raman spectrum of **TSB3,5-C₁₂** deposited on HOPG exhibits only one band at 1582 cm^{−1}, assigned to the G-band of graphite (Fig. S3a, ESI†). No peak from **TSB3,5-C₁₂** is detected since we are outside the absorption range (~350 nm) of this molecule. When **ZnPc** molecules are added into the **TSB3,5-C₁₂** templates, additional bands are clearly seen (Fig. S3b, ESI†). The positions of these bands are in agreement with those of the **ZnPc** powder (Fig. S3d, ESI†). Thanks to the resonance effect, we were able to detect the presence of **ZnPc** on HOPG, in the pores of the **TSB3,5-C₁₂** network. It is interesting to

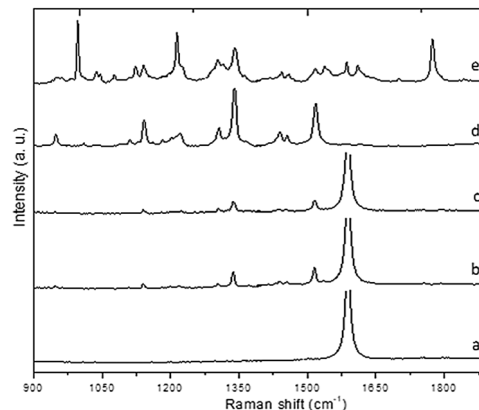


Fig. 3 Raman spectra (633 nm) of HOPG surfaces with deposits of (a) **TSB3,5-C₁₂**, (b) **TSB3,5-C₁₂** and **ZnPc**, and (c) **TSB3,5-C₁₂** and **ZnPc-L**. (d and e) The Raman spectra of pure **ZnPc** and pure ligand **L** powders, respectively.

note that in the literature, even at 633 nm, the Raman signal from **Pc** on HOPG is usually invisible.²⁷ When **ZnPc-L** molecules are added into the **TSB3,5-C₁₂** templates, the spectrum (Fig. S3c, ESI†) is similar to the one obtained after **ZnPc** addition. Thus, the Raman signature of the ligand **L** is not observed, even the intense bands at 1774, 1213, and 997 cm^{−1} (Fig. 3). Then, to understand this result, simulated Raman spectra of **ZnPc-L** at 633 nm wavelength excitation were computed (see the ESI† for calculation details, geometries, and spectra). The DFT calculations show that, if in the isolated **L** ligand, the symmetric stretching of C=O bonds ($\tilde{\nu} \sim 1780$ cm^{−1}) is one of the normal modes of the molecule with the highest Raman activity below 3000 cm^{−1}, it is no longer true in **ZnPc-L**. Indeed, in the complex, the Raman activity of this normal mode appears about several hundred times lower than that of the normal mode at $\tilde{\nu} \sim 1520$ cm^{−1} originating from the **Pc** moiety. Therefore, it is not surprising that the C=O band could not be observed even *via* resonance Raman spectroscopy experiments for a surface concentration below the monolayer range. The main result of the resonance Raman investigations lies in the observation of the **ZnPc** signature. This means that its fluorescence is quenched by HOPG and consequently confirms that the **Pc** macrocycles lie flat on HOPG.

As deduced from the STM characterization and Raman spectroscopy, it is not possible to assure the presence of the ligand **L** on top of the **ZnPc** hosted inside the pores of the **TSB3,5-C₁₂** supramolecular network. Since the deposition of molecular species on a raw surface is known to change its physical properties, we finally decided to track the presence of ligand **L** by measuring the HOPG surface energy variations upon modification *via* our surface-confined host-guest approach. This is achieved by measuring the contact angle, θ , a quantitative measure of the wetting of a solid by a liquid.²⁸ Moreover, this macroscopic characterization is compatible with large area substrates. Here, the water contact angles (WCA) of bare HOPG and HOPG after the deposition of **TSB3,5-C₁₂**, **ZnPc**, and **ZnPc-L** were determined (Fig. S3 and Table S1, ESI†). The basal-plane HOPG is known to be slightly hydrophilic,²⁹ which is confirmed by the value of $\theta = 84.6^\circ \pm 0.8^\circ$. Depositing the non-polar **TSB3,5-C₁₂** molecules should increase the hydrophobicity and thus the WCA, as effectively observed ($\theta = 91.2^\circ \pm 1.4^\circ$). In contrast,

filing the pores of the **TSB3,5-C₁₂** network by subsequent addition of **ZnPc** molecules, soluble in polar solvents, should lead to a decrease of the WCA. This is experimentally confirmed, the contact angle being equal to $\theta = 85.7^\circ \pm 1.1^\circ$. Thus, angle contact measurement is sensitive enough to estimate the change in the HOPG surface state. Now, by trapping the **ZnPc-L** complex instead of **ZnPc** in the 2D porous template, a more significant change is observed as the WCA strongly decreases from $91.2^\circ \pm 1.4^\circ$ for the **TSB3,5-C₁₂** network to $78.1^\circ \pm 1.3^\circ$. These results demonstrate the filling of the pores by a species dissimilar to **ZnPc** that modifies drastically the hydrophilicity of the entire substrate. We can infer that this molecule is the 3D **ZnPc-L** complex, its elbow structure evidenced by modeling favoring the hydrophilicity. Indeed, the two C=O bonds are available for H-bonding with water molecules on the one hand, and, in addition, within this geometry, **ZnPc-L** was computed to have a permanent dipolar moment of 7.2 D on the other hand. Finally, the above hydrophilicity tuning demonstrates the HOPG functionalization.

To summarize, we have developed a new method to trap a functional 3D **ZnPc-L** complex into a large 2D nanoporous template. This facile process combines the surface-confined host-guest chemistry and drop-casting method. We describe an unusual approach relying on the large-scale observation of the functionalized surface allowing the use of several experimental techniques such as STM at the air/solid interface, resonance Raman spectroscopy, and contact angle measurements. By overlapping the different results, it is possible to reliably prove the controlled immobilization of the building block molecules at a long range. Due to the versatility of the ligand complex chemistry, our manipulable platform could be used for a new generation of clickable surfaces for potential applications in e.g. nanophotonics or biosensing.

This work was supported by the LabEx MiChem, part of French state funds managed by the ANR within the “Investissements d’Avenir” program under reference ANR-11-IDEX-0004-02 and the Global Research Laboratory (GRL) through the National Research Foundation of Korea (NRF) funded by the Ministry of Science, ICT & Future Planning (no. 2016K1A1A2912753). We thank Y. Berger (MONARIS) for his helpful technical support.

Conflicts of interest

There are no conflicts to declare.

Notes and references

- J. Barth, G. Costantini and K. Kern, *Nature*, 2005, **437**, 671; C.-A. Palma, M. Cecchini and P. Samori, *Chem. Soc. Rev.*, 2012, **41**, 3713; S. Mali, J. Adisoejoso, E. Ghijsens, I. De Cat and S. De Feyter, *Acc. Chem. Res.*, 2012, **45**, 1309.
- T. Yokoyama, S. Yokoyama, T. Kamikado, Y. Okuno and S. Mashiko, *Nature*, 2001, **413**, 619; S. De Feyter and F. C. De Schryver, *J. Phys. Chem. B*, 2005, **109**, 4290.
- L. Sosa-Vargas, E. Kim and A. J. Attias, *Mater. Horiz.*, 2017, **4**, 570; J. A. A. W. Elemans, S. B. Lei and S. De Feyter, *Angew. Chem., Int. Ed.*, 2009, **8**, 7298.
- D. Bonifazi, S. Mohnani and A. Llanes-Pallas, *Chem. – Eur. J.*, 2009, **15**, 7004; T. Kudernac, S. Lei, J. A. A. W. Elemans and S. De Feyter, *Chem. Soc. Rev.*, 2009, **38**, 402; J. Teyssandier, S. De Feyter and K. S. Mali, *Chem. Commun.*, 2016, **52**, 11465.
- S. Stepanow, M. Lingenfelder, A. Dmitriev, H. Spellmann, E. Delvigne, N. Lin, X. Deng, C. Cai, J. V. Barth and K. Kern, *Nat. Mater.*, 2004, **3**, 229; H. L. Zhang, W. Chen, H. Huang, L. Chen and A. T. S. Wee, *J. Am. Chem. Soc.*, 2008, **130**, 2720; M. Blunt, X. Lin, M. d. C. Gimenez-Lopez, M. Schroder, N. R. Champness and P. H. Beton, *Chem. Commun.*, 2008, 2304.
- J. Adisoejoso, K. Tahara, S. Okuhata, S. Lei, Y. Tobe and S. De Feyter, *Angew. Chem., Int. Ed.*, 2009, **48**, 7353.
- G. Schull, L. Douillard, C. Fiorini-Debuisschert, F. Charra, F. Mathevet, D. Kreher and A. J. Attias, *Nano Lett.*, 2006, **6**, 1360.
- K. Tahara, K. Nakatani, K. Iritani, S. De Feyter and Y. Tobe, *ACS Nano*, 2016, **10**, 2113.
- K. Tahara, K. Inukai, J. Adisoejoso, H. Yamaga, T. Balandina, M. O. Blunt, S. De Feyter and Y. Tobe, *Angew. Chem., Int. Ed.*, 2013, **52**, 8373.
- X. Zhang, Y. Shen, S. Wang, Y. Guo, K. Deng, C. Wang and Q. Zeng, *Sci. Rep.*, 2012, **2**, 742.
- M. O. Blunt, J. C. Russell, M. d. C. Gimenez-Lopez, N. Taleb, X. Lin, M. Schröder, N. R. Champness and P. H. Beton, *Nat. Chem.*, 2011, **3**, 74.
- B. Baisch, D. Raffa, U. Jung, O. M. Magnussen, C. Nicolas, J. Lacour, J. Kubitschke and R. Herges, *J. Am. Chem. Soc.*, 2009, **131**, 442; M. Hammerich, T. Rusch, N. R. Krekieleh, A. Bloedorn, O. M. Magnussen and R. Herges, *ChemPhysChem*, 2016, **17**, 1870.
- P. Du, M. Jaouen, A. Bocheux, C. Bourgogne, Z. Han, V. Bouchiat, D. Kreher, F. Mathevet, C. Fiorini-Debuisschert, F. Charra and A.-J. Attias, *Angew. Chem., Int. Ed.*, 2014, **53**, 10060; S. Le Liepvre, P. Du, D. Kreher, F. Mathevet, A.-J. Attias, C. Fiorini-Debuisschert, L. Douillard and F. Charra, *ACS Photonics*, 2016, **3**, 2291.
- J. M. Gottfried, *Surf. Sci. Rep.*, 2015, **70**, 259.
- T. Ye, T. Takami, R. Wang, J. Jiang and P. S. Weiss, *J. Am. Chem. Soc.*, 2006, **128**, 10984; W. Auwärter, D. Écija, F. Klappenberger and J. V. Barth, *Nat. Chem.*, 2015, **7**, 105.
- O. P. H. Vaughan, F. J. Williams, N. Bampas and R. M. Lambert, *Angew. Chem., Int. Ed.*, 2006, **45**, 3779; J. Visser, N. Katsonis, J. Vicario and B. L. Feringa, *Langmuir*, 2009, **25**, 5980.
- D. Bleger, D. Kreher, F. Mathevet, A. J. Attias, G. Schull, A. Huard, L. Douillard, C. Fiorini-Debuisschert and F. Charra, *Angew. Chem., Int. Ed.*, 2007, **46**, 7404; G. Schull, L. Douillard, C. Fiorini-Debuisschert, F. Charra, F. Mathevet, D. Kreher and A. J. Attias, *Adv. Mater.*, 2006, **18**, 2954; C. Arrigoni, G. Schull, D. Bléger, L. Douillard, C. Fiorini-Debuisschert, F. Mathevet, D. Kreher, A.-J. Attias and F. Charra, *J. Phys. Chem. Lett.*, 2010, **1**, 190.
- G. Schull, PhD thesis, École normale supérieure de Cachan, 2006.
- T. Inose, D. Tanaka, O. Ivasenko, K. Tahara, S. De Feyter, Y. Tobe, H. Tanaka and T. Ogawa, *Chem. Lett.*, 2016, **45**, 286.
- D. P. Nair, M. Podgórski, S. Chatani, T. Gong, W. Xi, C. R. Fenoli and C. N. Bowman, *Chem. Mater.*, 2014, **26**, 724; A. D. Baldwin and K. L. Kiick, *Bioconjugate Chem.*, 2011, **22**, 1946.
- S. K. Sinha and S. K. Shrivastava, *Bioorg. Med. Chem. Lett.*, 2013, **23**, 2984.
- H. Wurm, W. Regel and M. L. Hallensleben, *Makromol. Chem.*, 1979, **180**, 1581; F. Severini, M. Pegoraro, G. Ricca, G. Audisio, D. Dainese and R. Gallo, *Polym. Int.*, 1990, **23**, 23.
- J. Köttleritzsch, S. Stumpf, S. Hoepfner, J. Vitz, M. D. Hager and U. S. Schubert, *Macromol. Chem. Phys.*, 2013, **214**, 1636.
- R. Díaz-Torres and S. Alvarez, *Dalton Trans.*, 2011, **40**, 10742.
- P. Kasprzycki, L. Sobotta, S. Lijewski, M. Wierzchowski, T. Goslinski, J. Mielcarek, C. Radzewicz and P. Fita, *Phys. Chem. Chem. Phys.*, 2017, **19**, 21390.
- M. E. El-Khouly and S. Fukuzumi, *Photochem. Photobiol. Sci.*, 2016, **15**, 1340; Y. Rio, W. Seitz, A. Gouloumis, P. Vázquez, J. L. Sessler, D. M. Guldi and T. Torres, *Chem. – Eur. J.*, 2010, **16**, 1929.
- X. Ling, L. Xie, Y. Fang, H. Xu, H. Zhang, J. Kong, M. S. Dresselhaus, J. Zhang and Z. Liu, *Nano Lett.*, 2010, **10**, 553.
- D. Y. Kwok, T. Gietzelt, K. Grundke, H.-J. Jacobasch and A. W. Neumann, *Langmuir*, 1997, **13**, 2880.
- Y. Wei and C. Q. Jia, *Carbon*, 2015, **87**, 10.